RESONATOR DESIGN CONSIDERATIONS FOR EFFICIENT OPERATION OF SOLID-STATE LASERS END-PUMPED BY HIGH-POWER DIODE-BARS

W. A. CLARKSON AND D. C. HANNA
Optoelectronics Research Centre
University of Southampton
Southampton, SO17 1BJ
United Kingdom

Abstract

A novel resonator design strategy for high-power diode-end-pumped solid-state lasers is described, which reduces the beam distortion and depolarisation loss due to thermally-induced lens aberrations and stress-birefringence. The approach is based on a resonator design satisfying two criteria: firstly, the laser mode radius must be appreciably smaller than the pump beam radius, and secondly, the laser mode size must decrease with decreasing power (increasing focal length) of the thermal lens. Experimental results are presented for diode-bar-pumped Nd:YAG lasers operating at various wavelengths confirming the validity of this approach. Results are also presented of a detailed investigation of thermal effects in end-pumped Nd:YAG lasers, which indicate how the various factors such as end-face curvature and the temperature and stress dependence of refractive index influence the thermal lensing behaviour. The merits of Nd:YLF for use in high-power end-pumped lasers, based on its weaker thermal lensing on the σ polarisation at 1.053μm compared to Nd:YAG, will also be considered.

1. Introduction

Advances in semiconductor laser technology over the last decade have been dramatic, leading to a very significant increase in the available output power from diode-bar sources. In parallel with these developments there has been growing interest in using high-power diode-bars as pump sources for power-scaling of solid-state lasers. At relatively low pump powers (< few watt), the employment of end-pumped rather than side-pumped configurations has been the preferred route owing to the much higher efficiencies achievable, the relative ease with which fundamental transverse mode operation can be selected and the enormous flexibility in cavity design and wavelength of operation. This has enabled the development of numerous novel solid-state laser devices (e.g. [1],[2]). Many of these attractive features result directly from the relative

R. Kossowsky et al. (eds.), Optical Resonators – Science and Engineering, 327–361.
© 1998 *Kluwer Academic Publishers. Printed in the Netherlands.*

ease with which low power diodes can be focused to small beam sizes, and their relatively narrow emission linewidths allowing short absorption lengths, ~few mm, in the laser material.

Progress in scaling diode-end-pumped solid-state lasers to high powers, whilst retaining these attractive features, has been hindered by two main problems. The first of these has been the unfriendly and highly elliptical nature of the output beams from high-power diode-bars. Typically, these devices are constructed from a wide array of emitters, with typical overall dimensions $\sim 1\mu m \times 10mm$ and, as a consequence, produce an output beam which is nearly diffraction-limited in the plane perpendicular to the array, but is typically ~2000 times diffraction-limited in the array plane. This large mismatch in the M^2 beam quality factors for orthogonal planes makes it difficult to focus to the small diameter beams required for efficient end-pumping of solid-state lasers.

To permit focusing to small beam diameters it is necessary to use an optical beam delivery system which equalises the beam quality factors in orthogonal planes without significantly decreasing the brightness. To date, a number beam delivery schemes which attempt to solve this problem have been reported (e.g. coupling into optical fibre bundles [3],[4],[5], using diffractive optical components [6] or using arrays of micro-optical components [7]). However, in most cases the equalisation in the beam quality factors is also accompanied by a large decrease in brightness. More recently, an alternative beam shaping technique [8] which allows equalisation of the beam quality factors in orthogonal planes with only a relatively small reduction in brightness has been demonstrated. This approach which utilises two high reflectivity mirrors in combination with standard collimating and focusing lenses can be used to focus the output from a diode bar to a nearly circular spot of much smaller diameter than is currently possible via other reported techniques, and hence offers the attractive prospect of efficient high-power operation even on relatively low gain or quasi-three-level transitions [9].

However, the availability of high power and high intensity pump sources has further exacerbated thermal effects such as thermal lensing and thermally-induced stress-birefringence, which are particularly pronounced in end-pumped lasers owing to the high thermal loading density. One of the main problems encountered in end-pumped lasers is beam distortion due to the highly aberrated thermal lens, making it extremely difficult to simultaneously achieve high efficiency and good beam quality. To overcome this problem a number of approaches have been reported including the use of apertures to select the TEM_{oo} beam [1], and aspheric lenses as compensators [2]. More recently, an alternative approach has been reported [10], which uses face-cooling to achieve axial heat flow in a laser disc and hence a significant decrease in the strength of the thermal lensing. Unfortunately, the latter approach has the disadvantage that it is only applicable to laser materials with a short absorption length for the pump light and/or laser transitions with a high gain cross-section. This is necessary to ensure that the pumped region has a high aspect ratio of pump beam size to disc thickness to minimise radial heat flow.

In this paper we describe an alternative resonator design strategy to reduce the beam distortion resulting from strong thermally-induced aberrations without using

compensating components. The underlying basis of this approach is that the aberrations which result from the Gaussian-like pump beam are most pronounced in the wings of the inversion distribution. Hence by using a resonator with a TEM_{oo} mode which is smaller than the pump beam it is possible to achieve a near-diffraction-limited output beam. However, a consequence of the smaller mode size is that it is more difficult to achieve efficient extraction of the gain stored in the wings of the inversion distribution. In addition, appropriate measures must be taken to prevent this unused inversion from providing sufficient gain for simultaneous oscillation on higher-order transverse modes. Our results indicate that this suppression of higher-order transverse modes can be achieved by applying a second condition to the resonator design, namely that the TEM_{oo} beam size in the laser rod should decrease with increasing focal length of the thermal lens. The rationale for this design is presented below. Experimental results for diode-bar-pumped Nd:YAG lasers operating at various wavelengths which confirm the benefits of this approach are described together with a results of a detailed investigation of thermal effects in Nd:YAG which indicate how various factors, such as end-face curvature and the temperature and stress-dependence of the refractive index influence the thermal lensing behaviour and hence the choice of resonator design. In addition, the merits of Nd:YLF with its weaker thermal lensing on the 1.053μm polarisation compared to Nd:YAG for use in high-power end-pumped lasers will be considered.

2. Resonator Design Considerations For Low-power Lasers

We begin our discussion with a brief review of the resonator design criteria for efficient TEM_{oo} operation of diode-pumped solid-state lasers at low powers [11],[12]. Using a simplified rate equation approach [13], and assuming Gaussian transverse intensity distributions for the pump beam and lasing mode, the following approximate expressions for threshold pump power P_{pth} and slope efficiency η_s of an end-pumped laser (fig.1) can be derived [14]:

$$P_{pth} = \frac{\pi h \nu_p (L+T)(w_p^2 + w_L^2)}{4\sigma\tau_f \eta_q \eta_{abs}} \qquad (1)$$

and

$$\eta_s = \left(\frac{T}{L+T}\right)\left(\frac{\nu_p}{\nu_L}\right)\eta_{abs}\eta_q\eta_{PL} \qquad (2)$$

where ν_p and ν_L are the pump and lasing frequencies respectively, τ_f is the fluorescence lifetime, σ is the laser transition cross-section, η_q is the pumping quantum efficiency

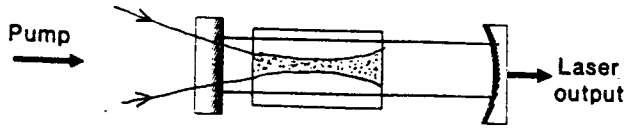

Figure 1 End-pumped solid-state laser.

(i.e. the fraction of absorbed pump photons which lead to subsequent excitation in the upper laser level), T is the transmission of the output coupler, L is the residual round-trip cavity loss, $\eta_{abs} \approx [1-\exp(-\alpha_p l)]$ is the fraction of incident pump radiation absorbed over the length of the laser rod and w_L and w_p are the effective TEM_{oo} beam radii for laser and pump respectively, which are assumed to be approximately constant over the length of the laser rod. The above expressions for threshold and slope efficiency also assume that the total cavity loss $(L+T) << 1$, which is usually a reasonable approximation for most low power diode-pumped lasers. The factor η_{PL} depends on the spatial overlap of the pumped region and lasing mode and on the ratio of the intracavity intensity, I to the saturation intensity, $I_s \approx h\nu_L/\sigma\tau_f$. In the low power limit where $I/I_s \ll 1$, then η_{PL} can be approximated to

$$\eta_{PL} \approx \frac{w_L^2 (w_L^2 + 2w_p^2)}{(w_L^2 + w_p^2)^2} \tag{3}$$

and at higher powers where $I/I_s \gg 1$, $\eta_{PL} \rightarrow 1$. Thus η_{PL} accounts for the variation in the slope efficiency with pump power. Physically, this can be interpreted as being due to a competition between stimulated emission and spontaneous emission in the wings of the pumped region. At high intracavity intensities there is an increased probability that inverted ions will be depleted by stimulated emission and hence an increase in the slope efficiency. The fact that the slope efficiency is power dependent makes it difficult to calculate the optimum output coupling for maximum output power from the laser (i.e. for maximum output power). However, if it is assumed that $\eta_{PL} \approx 1$, which is usually a good approximation for an optimally designed laser at low pump powers, then the optimum value for the output coupler transmission can be chosen according to the following equation:

$$T = -L + 2\sqrt{\frac{P_p \sigma \tau_f \eta_{abs} \eta_q L}{\pi (w_L^2 + w_p^2) h\nu_p}} \tag{4}$$

where P_p is the maximum pump power available and it has been assumed that

$(L+T) \ll 1$. Thus equations (1) to (4) provide a good guide to the optimum laser design. For a given laser transition the key requirement for efficient operation is a low threshold compared to the available pump power, which can generally be achieved by keeping the net cavity losses low and using small pump beam and laser mode sizes. The laser mode size is determined by the resonator design and can in general be made very small. To ensure diffraction-limited operation it is necessary to use a resonator design in which the TEM_{∞} radius is either equal to or, more ideally, larger than the pump beam radius. This prevents undepleted inversion from building up in the wings of the pumped region which may result in lasing on higher-order transverse modes. Thus the minimum laser mode size, and hence the minimum threshold pump power is determined mainly by the minimum effective pump beam size, which is in turn governed by the M^2 beam quality factor for the diode laser, the performance of the pump collimating and focusing optics and the absorption length α_p for the pump light. If we make the simplifying assumption that the pump light is absorbed linearly with distance z and is completely absorbed over two absorption lengths, then minimum effective pump beam radius w_{pmin}, defined as r.m.s beam radius which results in the minimum pumped volume, is given by

$$w_{pmin}^2 = \frac{2\lambda M^2}{\alpha_p \pi n \sqrt{3}} \qquad (5)$$

For most diode laser pump sources the beam quality factors differ considerably for orthogonal planes. In the plane perpendicular to the junction the beam quality factor M_y^2 is ~ 1. In the orthogonal plane parallel to the array the beam quality factor M_x^2 is much larger and depends on the length of the array. For a typical 1W diode laser at 809nm the emitting region has a length $\sim 200\mu m$ and produces a beam with $M_x^2 \sim 40$, suggesting a minimum effective pump beam radius of approximately $130\mu m$ for a Nd:YAG rod with a typical absorption length for the pump of $\approx 2.5mm$. This pump beam size can be achieved rather easily with a standard arrangement of lenses. Obviously, a much smaller effective pump beam size is possible in the orthogonal plane. However, since it is generally much easier to design a resonator with a nearly circular TEM_{∞} mode, then clearly it is the larger of the pump beam's M^2 values which determines the laser mode radius and hence the minimum threshold pump power. Assuming a residual round-trip cavity loss L of 2% (due to imperfect antireflection coatings and leakage through the high reflector) we can estimate from equation (4) that the optimum output coupler transmission for operation at $1.064\mu m$ will be $\sim 13\%$, which would result in a threshold pump power of $\sim 125mW$ and a maximum output power of around 400mW to 500mW in a diffraction-limited beam. These operating characteristics are fairly typical of low-power diode-pumped Nd:YAG lasers. For quasi-three-level lasers the above analysis must be modified to account for the finite lower laser level population [15],[16]. However, the design strategy is essentially the same with the laser performance on a given transition being determined mainly by how

tightly the diode pump beam can be focused in the laser material. In fact it is a consequence of ability to focus the pump beam to a diameter which is much smaller than the absorption length which enables end-pumped solid-state lasers to be significantly more efficient than side-pumped lasers. The relatively weak thermal effects in low-power diode-pumped lasers in combination with the relative ease with which the requirement of $w_L \geq w_p$ for TEM_{oo} operation can be achieved, has allowed for considerable flexibility in the resonator design, of which there are numerous examples reported in the literature.

3. Focusing of High-power Diode Lasers

Due to thermal considerations scaling of diode laser pump sources to higher powers has been achieved via the construction of longer linear arrays of lower power diodes, and hence has been accompanied by a degradation in beam quality and a decrease in brightness. A typical commercially available 20W cw diode-bar at 809nm has a linear array of dimensions $\sim 1\mu m \times 10mm$ and very different beam quality factors in orthogonal planes; $M_y^2 \sim 1$ and $M_x^2 \sim 2000$. By comparison with a typical 1W diode laser, a typical 20W diode-bar has a brightness at least 2.5 times smaller. Whilst this reduction in brightness is of some significance, by far the most serious problem for end pumping is the large difference in the M^2 values for orthogonal planes. This makes it extremely difficult to focus to the small diameter beam required for efficient end-pumping. A number of beam delivery schemes which attempt to solve this problem have been reported (e.g. [5],[6],[7]). However, equalisation of the M^2 values in orthogonal planes is often accompanied by a significant decrease in brightness thus precluding the small focussed beam sizes required for efficient end-pumping of low gain or quasi-three-level lasers.

In the experimental investigations described in this work we have made use of an alternative technique which utilises only two high reflectivity mirrors to equalise the M^2 values in orthogonal planes without a significant decrease in brightness. The principle of operation of this 'two-mirror' beam shaping technique is described in detail in ref.[8]. Here we merely summarise its main features:

The construction of the two-mirror beam shaper (shown in the Figs. 2(a) and (b)) is very simple, with the two high reflectivity plane mirrors aligned approximately parallel and separated by a small distance d (typically $< 1mm$). The mirrors are transversely offset from each other, in both the x′ and y′ directions, so that small sections of each mirror are not obscured by the other. These unobscured sections form the input and output apertures of the beam shaper.

The principle of operation of the beam shaper can be explained with reference to Figs. 2(a) and (b), which show, respectively, plan and side views of the beam shaper, in each case the mirror surfaces being orthogonal to the plane of the figure. Light from a non-diffraction-limited laser (in this case a diode-bar) with beam quality factors M_x^2 and M_y^2 in orthogonal planes of propagation x-z and y-z, is incident obliquely at angles $\theta_{x'}$ and $\theta_{y'}$ in the orthogonal planes; x′-z′ and y′-z′, on the unobscured section of mirror

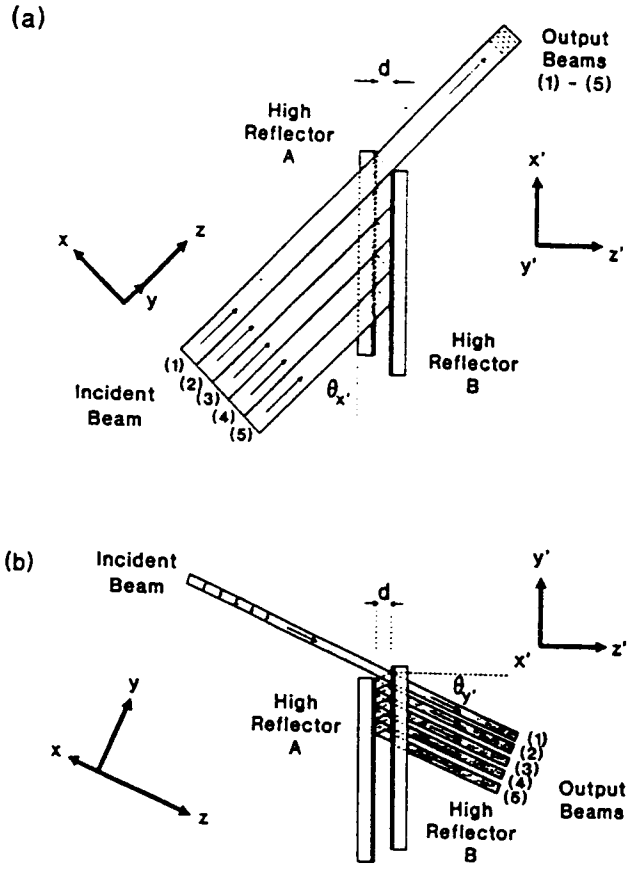

Figure 2 Two-mirror beam shaper, (a) plan view, (b) side view.

B of the beam shaper as shown. The incident beam can be considered to be composed of a number of adjacent beams. For the purpose of illustration, the incident beam has been arbitrarily chosen to consist of five parallel beams (1)-(5). Beam (1) is not incident on either mirror A or B, since it passes above mirror A (see Fig. 2(b)) and passes by the side of mirror B (see Fig. 2(a)), and so emerges with no change to its original direction (assuming any diffraction effects at the edge of mirror B are negligible). Beam (2) however, passes above mirror A but is incident on mirror B and is reflected so that it strikes mirror A immediately below beam (1). Beam (2) is then reflected at mirror A and emerges from the beam shaper in the direction of beam (1), but displaced beneath beam (1). Beam (3), after incidence on mirror B, is reflected so that it strikes mirror A underneath beam (2), is then reflected back to mirror B, where

it is reflected onto mirror A, subsequently emerging parallel to beams (1) and (2) but displaced underneath beam (2). Beams (4) and (5) undergo similar multiple reflections at mirrors A and B and finally emerge propagating beneath beams (1), (2) and (3), as shown in Fig. 2(b). Thus the action of the beam shaper is to effectively chop the incident laser beam into a specific number of beams and then to re-direct and re-position these beams so that they emerge from the beam shaper stacked on top of one another. Since the incident beam is initially many times diffraction-limited in the x-z plane (i.e. $M_x^2 \gg 2000$ for a typical diode bar), then the effect of the beam shaper is to decrease the width of the beam in the x direction, but without significantly increasing its divergence. Thus the overall result is that the composite beam which emerges from the beam shaper has a smaller value for M_x^2. For a given incident laser beam, the number of stacked beams and their widths (in the x-z plane) can be specified by the choice of angles $\theta_{x'}$ and $\theta_{y'}$, the mirror separation d and by the appropriate positioning of the beam shaper relative to the incident laser beam. Hence the factor by which M_x^2 is reduced can be controlled by the adjustment of these parameters. It should be noted however, that a reduction in M_x^2 is only possible if M_x^2 for the incident beam is much greater than unity so that chopping the beam into smaller individual beams does not result in an increased spread of these beams due to diffraction at the edge of mirror B.

In the y direction the beam size is increased, but the divergence remains approximately constant (providing that mirrors A and B are sufficiently parallel), hence the emerging beam has its M_y^2 value increased. The factor by which M_y^2 is increased depends on the total height of the composite stacked beam (in the y-z plane) and its far-field divergence. If the incident beam is reasonably well collimated in the y-z plane then M_y^2 is increased by a factor approximately equal to the total height of the emerging beam divided by the height of an individual beam. For many applications, it is desirable to minimise the increase in M_y^2 by choosing values for the mirror spacing d, and the inclination angle $\theta_{y'}$ so that the gap between adjacent stacked beams is minimised without significantly degrading the beam shaper's transmission due to clipping of the beams at the top edge of mirror A. For a clipping loss of $<1\%$, the beam separation should be ~ 1.3 times greater than the $1/e^2$ incident beam height. This implies that M_y^2 would be increased by a factor of $\sim 1.3N$, where N is the number of stacked beams.

The factor by which M_x^2 is decreased depends on the width of the output beam (in the x-z plane) and its far-field divergence. As a rough guide, it should be possible to decrease M_x^2 by a factor $\sim N$ (providing that the initial value for M_x^2 is much greater than N).

The transmission T of the beam shaper is approximately given by $T=(1-L)[1-N(1-R)]$ where L is the loss due to clipping and R is the mirror reflectivity. If the incident beam is chopped many times, then many reflections are needed between the mirrors, so high reflectivity is important for achieving a high transmission.

Thus, by choosing appropriate values for the mirror separation d and inclination angles; $\theta_{x'}$ and $\theta_{y'}$, it is, in principle, possible to re-configure any non-diffraction-limited laser beam with $M_x^2 \gg M_y^2$ so that M_x^2 is made approximately equal to M_y^2, with only a very small reduction in brightness. The resulting beam can then be focused with

conventional lenses to a nearly circular spot which is suitable for end-pumping.

The beam delivery scheme used in the end-pumping experiments described here is shown in fig. 3. The pump was a 20W cw diode-bar (Opto-Power-Corporation OPC-A020-mmm-CS) with 24 emitters which was initially collimated by a fibre lens and then imaged with an arrangement of cylindrical and spherical lenses, which were positioned so to produce a magnified image of the array of emitters at the entrance aperture to the two-mirror beam shaper. The beam shaper itself was constructed as shown in fig. 2 with two nominally parallel high reflectivity mirrors ($>99.8\%$ at the diode wavelength, ~ 808nm), and was inclined at angle $\theta_{x'} \approx 45°$ with respect to the incident beam. The mirror separation d and the inclination angle $\theta_{y'}$ were adjusted in order to chop the incident beam into 24 constituent beams, one for each emitter, and stack them vertically below each other in the y direction. In general the choice of parameters d and $\theta_{y'}$, and therefore the number of stacked beams, depends on the required output values of M_x^2 and M_y^2. However, in the case of a diode bar, with its array of emitters, it is often advantageous to image the bar onto the beam shaper and configure the beam shaper to chop the beam into its constituent emitter images. In this way it is possible to effectively remove the 'dead' space between adjacent emitters on the bar and in so doing increase the brightness. The increase in brightness depends on the ratio of the emitter width to the dead space width (i.e. the fill factor), and is approximately a factor of two for the diode bar used in our experiments. The stacked output from the beam shaper was then re-collimated in the x-z plane by a cylindrical lens of focal length 200mm and finally focused with an appropriate spherical lens selected to give the required spot size. The resulting beam quality factors, M_x^2 and M_y^2 depend on the alignment of the beam shaper and on the initial values of M_x^2 and M_y^2 at the diode bar. Thus there is some variation in performance depending on the details of the actual set-up. In an optimised arrangement, final M^2 beam quality factors of ~ 40 in orthogonal planes have been achieved, although M^2 values in the range 60 to 70 are more typical. The overall transmission of the focusing scheme is typically $\sim 75\%$, resulting in ~ 15W of available pump power at the focus.

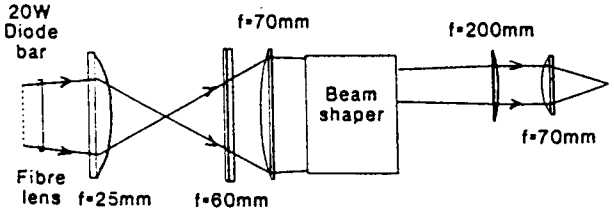

Figure 3 Focusing arrangement for a 20W diode bar

4. Prospects For Power-scaling End-pumped Lasers

Based on the focusing scheme performance described above we can estimate the threshold and output power of end-pumped solid-state lasers using this pumping arrangement from equations (1)-(4). From equation (5), the minimum effective pump beam size w_{pmin} for a pump source with $M_x^2=M_y^2=70$ is $\sim 184\mu m$. Hence for a Nd:YAG laser operating at $1.064\mu m$ with an output coupler transmission of 10% and an additional round-trip loss of 2% we predict a threshold pump power of $\sim 0.2W$ and, by making $\eta_{PL}\rightarrow 1$ using $w_L > w_p$ (say $250\mu m$), a maximum TEM_{oo} output power of $\sim 8W$ for 15W of incident pump power should in principle be achievable. In addition, since the threshold pump power is very much smaller than the maximum available pump power, it should be possible to operate at a multiwatt power levels on laser transitions with a $\sigma\tau_f$ product which is more than an order of magnitude smaller, as well as on many quasi-three-level transitions. Thus, the high brightness output from this diode-bar end-pumping scheme appears to offer an attractive route to power-scaling of numerous solid-state lasers.

5. Thermal Effects in Continuous-wave End-pumped Lasers

The predictions for laser performance described in the previous section are extremely difficult to realise in practice due to thermal effects which are particularly pronounced in end-pumped lasers owing to the high thermal loading density. The main origin of heat generation in diode-pumped lasers is usually considered to be quantum defect heating, i.e. simply due to the energy difference between pump and emitted photon [17]. In addition, for many laser transitions there are a number of other mechanisms (e.g. upconversion and excited-state absorption) which may also lead to significant extra heat loading. The heat generated results in a spatial variation in temperature, and consequently internal stresses within the laser material, and in addition, deformation of the laser rod end faces due to differential expansion. The net result is a degradation in laser beam quality due to thermal lensing, depolarisation loss due to stress-induced birefringence, and ultimately fracture of the laser rod, if the thermally-induced stress exceeds the tensile strength of the laser material. The relative extent to which these effects are detrimental to the laser performance depends on a number of factors including; the thermo-mechanical and thermo-optical properties of the laser material, the pumping geometry, the laser medium geometry and the heat-sinking arrangement. In the work described here we are restricting our consideration to end-pumped lasers with edge-cooled rods of cylindrical geometry. The attraction of edge cooling is the relative simplicity of its implementation, but due to the predominantly radial heat flow it has the disadvantage of strong thermal lensing. Face-cooling, on the other hand, offers much weaker thermal lensing, but is complicated by the need for multiple-passes of the pump beam [10] due to the short rods required for predominantly axial heat flow, and hence is only applicable to laser materials with a short absorption length for the pump and/or laser transitions with relatively high gain. The ultimate limit of power-scaling is posed

by the onset of thermally-induced stress-fracture. However, in laser materials such as Nd:YAG which has a relatively high fracture limit, it is usually thermal lensing and stress-induced birefringence which present the practical limit on diffraction-limited laser performance in end-pumped configurations. In fact, since there are numerous techniques for adequately compensating for stress-birefringence [17],[18] it is generally the case that thermal lensing is the major problem. In the case of laser materials such as Nd:YLF which have superior thermo-optical properties but inferior thermo-mechanical properties, it is thermally-induced fracture which is the most significant problem. Hence, when attempting to scale end-pumped Nd:YLF to high powers, it is necessary to take special precautions in order to avoid fracture, as will be described later.

For the present discussion we will consider the situation where thermal lensing is the major obstacle to power-scaling as is frequently the case for Nd:YAG lasers. There are two main problems which must be addressed. The first problem is that in many situations strong thermal lensing will be the major factor in determining the laser mode size, hence making it extremely difficult to design a resonator in which the laser mode size does not vary appreciably with pump power. If the mode size varies significantly so that the pump beam is no longer 'mode-matched' then higher-order transverse modes may lase, thus also leading to a degradation in beam quality. One solution to this problem is simply to design the laser to operate TEM_{∞} for only a small range of pump powers near the maximum available pump power, and then use an attenuator if it is necessary to vary the output power. The second, and certainly the most serious problem is the highly aberrated nature of the thermal lens which results from the Gaussian-like transverse intensity profile of the pump beam. This can lead to a very significant degradation in beam quality in end-pumped lasers. In many situations, it is this problem more than any other which represents the most significant obstacle to simultaneously achieving both high efficiency and a diffraction-limited TEM_{∞} output in high-power end-pumped lasers.

To enable the formulation of an appropriate resonator design strategy for achieving the optimum TEM_{∞} performance at high pump powers, it is necessary to first derive an approximate expression for the focal length of the thermal lens and determine the effect of the non-parabolic phase aberrations on beam quality. Consider an edge-cooled laser rod of radius a, length l mounted in a cooled copper heat-sink maintained a temperature T(a), end-pumped by a high-power diode-laser with incident pump power P_p and intensity $I_p(r)$, as shown in fig. 4. Under steady state conditions:

$$\nabla.\mathbf{h}(r,z)=Q(r,z) \qquad (6)$$

where $\mathbf{h}(r,z)$ is the heat flux and $Q(r,z)$ is the power per unit volume deposited as heat in the laser medium. The heat flux gives rise to a temperature distribution $T(r,z)$ within the laser rod given by

$$\mathbf{h}(r,z) = -K_c \nabla T(r,z) \tag{7}$$

where K_c is the thermal conductivity of the laser material. Assuming that the thermal conductivity of the heat-sink is much larger than for the laser material, which would typically be the case (e.g. using a copper heat sink), then the temperature over the whole of the rod's circumference is T(a) and the heat flow is predominantly radial.

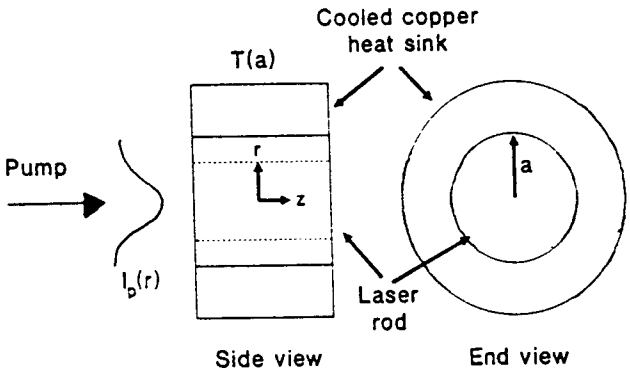

Figure 4 Heat sinking arrangement for an edge-cooled laser rod.

Hence from equation (6), the net radial heat flow from a thin disc, radius r and thickness Δz at axial position z is given by [19]

$$2\pi r \Delta z h(r,z) = \int_z^{z+\Delta z} \int_o^r 2\pi r' Q(r',z')\, dr'\, dz' \tag{8}$$

where h(r,z) is now the radial heat flux. If we make the simplifying assumptions that the ground state is not significantly depleted and that the pump beam radius w_p does not vary significantly over the pumped region of the laser rod, then Q(r,z) can be written:

$$Q(r,z) = \alpha_p \gamma I_p(r) \exp(-\alpha_p z) \tag{9}$$

where γ is the fraction of absorbed pump converted to heat. If the pumping quantum efficiency is unity and there are no deleterious upconversion or excited-state absorption processes, then under lasing conditions γ is approximately equal to the quantum defect (i.e. $\gamma \approx (\nu_p - \nu_L)/\nu_p$). Substituting (9) into (8) yields the following simplified expression for the radial heat flux h(r,z):

$$h(r,z) = \frac{\gamma \exp(-\alpha_p)}{r} \int_o^r I_p(r')\, dr' \tag{10}$$

The temperature difference $\Delta T(r,z) = T(r,z) - T(0,z)$ can be determined via substitution of (10) into (7), and the resulting phase difference $\Delta\phi(r) = \phi(0) - \phi(r)$ from

$$\Delta\phi(r) = \frac{2\pi}{\lambda} \int_o^l \Delta T(r,z) \frac{dn}{dT} dz \tag{11}$$

From equation (10) it can be seen that $\Delta T(r,z)$, $\Delta\phi(r)$, and hence the resulting beam distortion, depend on the transverse intensity distribution $I_p(r)$ of the pump beam. For high-power diode bars $I_p(r)$ has a transverse profile somewhere between Gaussian and'top-hat' depending on the output characteristics of the diode-bar and on the particular pump beam delivery scheme used. For the pump delivery scheme used in our experiments the pump intensity profile is better approximated to a Gaussian. However, to illustrate the importance of the pump beam profile and its effects on the thermal lensing we will consider both cases of 'top-hat' and Gaussian intensity profiles.

5.1. 'TOP-HAT' PUMP INTENSITY PROFILE

In the case of a uniform pump intensity $I_p = P_p/\pi w_p^2$ for $r \leq w_p$ and $I_p = 0$ for $r > w_p$, then from equations (7), (10) and (11) it can be show that the phase difference $\Delta\phi(r)$ is given by

$$\Delta\phi(r) = \left(\frac{P_p \gamma r^2 \eta_{abs} \frac{dn}{dT}}{2\lambda K_c w_p^2} \right) \tag{12}$$

for $r \leq w_p$, and

$$\Delta\phi(r) = \left(\frac{P_p \gamma \eta_{abs} \frac{dn}{dT}}{2\lambda K_c} \right) . \left[1 + 2 \log_e \left(\frac{r}{w_p} \right) \right] \tag{13}$$

for $r > w_p$. Hence the $\Delta\phi(r)$ increases quadratically with r for $r \leq w_p$ and logarithmically with r for $r > w_p$.

5.2. GAUSSIAN PUMP INTENSITY PROFILE

In the case of a pump beam with Gaussian intensity profile; $I_p(r) = (2P_p/\pi w_p^2)\exp(-2r^2/w_p^2)$, it can be shown that the phase difference $\Delta\phi(r)$ is given by

$$\Delta\phi(r) = \left(\frac{P_p \gamma \eta_{abs} \frac{dn}{dT}}{\lambda K_c} \right) . \left[-\sum_{n=1}^{\infty} \frac{1}{2nn!} \left(-\frac{2r^2}{w_p^2} \right)^n \right] \tag{14}$$

and hence $\Delta\phi(r)$ has a more complicated dependence on r which approximates to a quadratic dependence only when $r \ll w_p$.

In laser materials such as Nd:YAG the major contribution to thermal lensing arises from the temperature dependence of the refractive index, with the stress dependence of the refractive index and end-face bulging resulting in only relatively weak additional contributions to lensing, as will be seen later. Under these conditions the approximate focal length of the thermal lens f_t can be calculated by substituting the term in $\Delta\phi(r)$ which is quadratic in r into the following expression [19]:

$$f_t = \frac{\pi r^2}{\lambda \Delta\phi(r)} \qquad (15)$$

This assumes that the lens is a 'thin' lens (i.e. $1/\alpha_p \ll f_t$), which is usually a good approximation in end-pumped lasers. However, equation (15) only gives the focal length experienced by the central portion of the laser beam, and hence is of limited value in formulating a strategy for resonator design since it does not provide any information on the aberrated nature of the lens, or any means for estimating the degradation in laser beam quality. Hence, it is more appropriate to consider an aberrated thermal lens as one whose focal length varies radially. For a thin thermal lens with a given radially varying phase difference $\Delta\phi(r)$ an approximate expression for the focal length $f_t(r)$ can be derived from simple geometrical considerations (shown in fig.(5). The resulting expression is:

$$f_t(r) \approx \frac{2\pi r}{\lambda \dfrac{d\Delta\phi(r)}{dr}} \qquad (16)$$

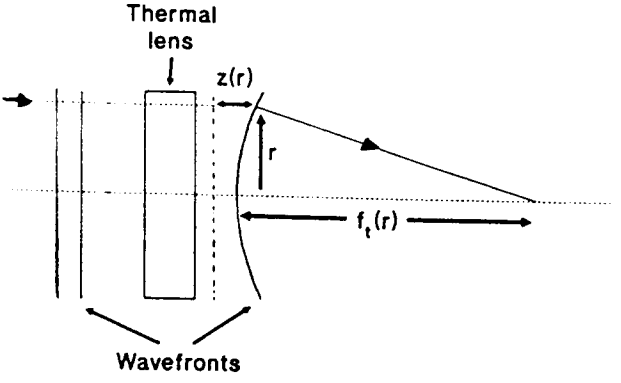

Figure 5 Radial variation in focal length for an aberrated thermal lens.

From equation (16) it can be seen that if $\Delta\phi \propto r^2$, then $f_t(r)$ is a constant and the lens has no phase aberration, and hence will not degrade the beam quality. For the 'top-hat' pump intensity profile described above, the focal length is given by

$$f_t(r) = \frac{2\pi K_c w_p^2}{P_p \gamma \eta_{abs} \frac{dn}{dT}} \qquad (r \leq w_p)$$

$$f_t(r) = \frac{2\pi K_c r^2}{P_p \gamma \eta_{abs} \frac{dn}{dT}} \qquad (r > w_p) \tag{17}$$

and for a Gaussian pump intensity profile the focal length is given by

$$f_t(r) = \frac{2f_t(0)}{w_p^2}\left(\frac{r^2}{1-\exp(-2r^2/w_p^2)}\right) \tag{18}$$

where $f_t(0)$ is the focal length on axis at $r=0$, given by

$$f_t(0) = \frac{\pi K_c w_p^2}{P_p \gamma \eta_{abs} \frac{dn}{dT}} \tag{19}$$

From the expressions for focal length (17), (18) and (19) we can compare the lens powers for 'top-hat' and Gaussian pump intensity profiles for otherwise identical operating conditions. The results of this comparison are shown in fig.6, where it can be seen that the thermal lensing on axis has a lens power that is a factor-of-two stronger for the Gaussian pump and is highly aberrated with only a small region in the centre ($r \ll w_p$) having essentially constant focal length. However the 'top-hat' pump beam, in addition to producing a much weaker lens on axis, produces a lens which is essentially unaberrated over the pumped region ($r \leq w_p$). For $r > w_p$ the lens power varies in a similar fashion for both Gaussian and 'top-hat' pump beams. Thus, the transverse intensity profile of the pump beam is a very important factor in determining the thermal lens power and its phase aberration. From fig. 6 it can be seen that in order to minimise the thermal lensing and beam distortion a 'top-hat' pump beam would be preferable to a Gaussian pump beam. However, a 'top-hat' pump beam has the disadvantage that the threshold pump power can be up to a factor-of-two higher, and the slope efficiency for TEM_{oo} operation can be significantly lower as the mode profile and inversion profile are less well matched. In any case, in practice it is very difficult to achieve a pump beam with a 'top-hat' transverse intensity profile without a significant loss in pump power. Hence it is more usual to simply accept whatever the pump

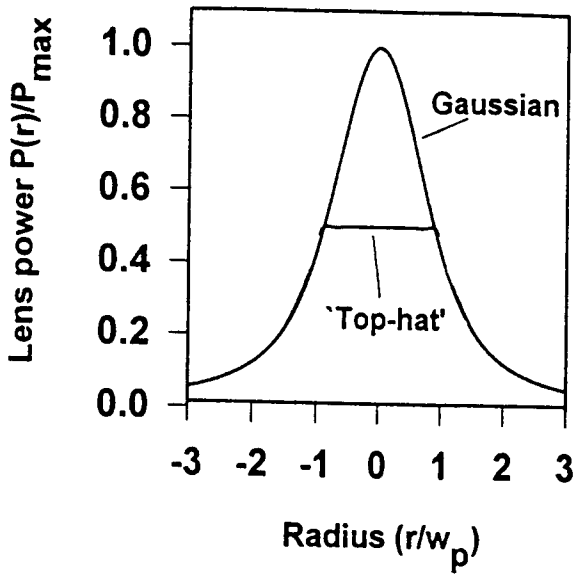

Figure 6 Predicted thermal lens power versus radius for Gaussian and 'top-hat' transverse pump intensity profiles.

delivery scheme provides and which is probably best approximated by a Gaussian transverse intensity distribution.

6. Measurement of Thermal Lensing

To test validity of this model we have determined the thermal lensing in a diode-pumped Nd:YAG rod, via a measurement of the phase difference as a function transverse position using a Mach-Zehnder interferometer. The experimental set-up (shown in fig.7), consisted of a 10mm long Nd:YAG rod, antireflection coated at the lasing wavelength (1.064μm) and the pump wavelength ($\sim$809nm), mounted in a water-cooled copper heat-sink, which was end-pumped by a 20W diode-bar. The diode-bar was focused, using a two-mirror beam shaping arrangement similar to that shown in fig. 3, to produce a nearly circular beam with radii; w_{px}=227μm and w_{py}=224μm and beam quality factors; $M_x^2 \approx 78$ and $M_y^2 \approx 63$ in orthogonal planes. This choice of beam size is representative of that required for efficient operation on some of the lower gain Nd:YAG transitions (e.g. at 946nm and 1.32μm). The pump beam was focused through a mirror coated for high reflectivity (>99.8%) at 1.064μm and high transmission (>95%) at 809nm at 45°incidence, resulting in a maximum of 14.2W of pump light

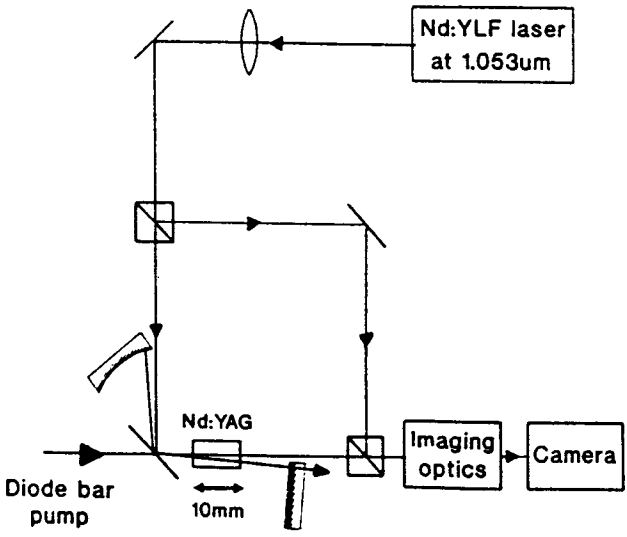

Figure 7 Mach-Zehnder interferometer for measuring the thermally-induced phase difference.

incident on the Nd:YAG rod. This mirror forms part of the Mach-Zehnder interferometer, allowing collinear propagation, along the pump beam's optical path, of the probe beam from a low-power diode-pumped single-frequency Nd:YLF ring laser operating at 1.053μm. The Nd:YLF laser was chosen to provide the probe beam because its 1.053μm output experiences negligible gain in the Nd:YAG. The output from the interferometer was imaged onto a CCD camera, which was used to monitor the resulting interference pattern, from which the phase difference was calculated. Since it was anticipated that there would be a difference in thermal loading under nonlasing and lasing conditions, the phase difference was measured under both operating conditions. Laser operation at 1.064μm was achieved using the simple three-mirror resonator show in fig.7, which was aligned non-collinearly at the smallest possible angle to the pump beam, whilst allowing the Nd:YLF probe beam unattenuated passage through the Nd:YAG rod. At the maximum pump power the laser produced ~6W of output in a multi-transverse-mode beam.

Under lasing conditions at the maximum available pump power, the measured phase difference as a function of radial position is shown in fig.8(a). The solid line in fig.8(a) is the parabolic curve which is the best fit to the phase difference data close to the centre of the pumped region. This indicates the phase difference profile that would be measured for a perfect (unaberrated) lens, and corresponds to a focal length of

$\approx$60mm. The deviation from the ideal parabolic phase difference profile, shown in fig. 8(b), reveals the highly aberrated nature of the thermal lens with the phase aberration becoming increasingly pronounced for $r > w_p$. The resulting radial variation in focal

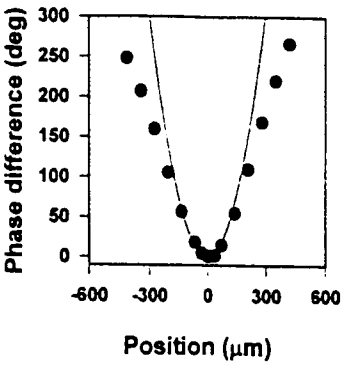

Figure 8(a) . Phase difference as a function of radial position under lasing conditions.

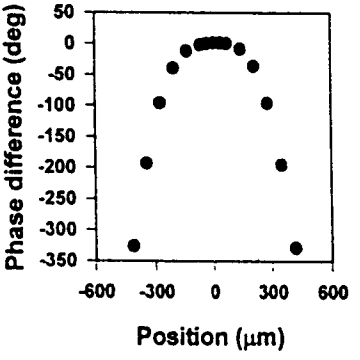

Figure 8(b) Deviation of phase difference from the ideal parabolic phase difference profile.

length can be calculated from the experimental data using equation (16), and compared with predicted variation in focal length for a Gaussian pump beam given by equation (18), where it is assumed that $K_c = 13 Wm^{-1}K^{-1}$, $dn/dT = 9.86 \times 10^{-6} K^{-1}$ for YAG [20], $\gamma \approx 0.32$ [21] for 1.064μm operation, $w_p = 235\mu m$, and $\eta_{abs} = 0.94$ The result of this comparison is shown in fig. 9, where the predicted values for focal length (dashed line) correspond to a slightly weaker lens than was measured in practice. This can be easily explained since the theoretical model takes into account the contribution to lensing which

arises only from the temperature dependence of the refractive index, whereas the experimental values for focal length also include the contributions arising from end-face bulging and the radial stress dependence of the refractive index. From independent measurements of the stress-induced birefringence, using the Mach-Zehnder

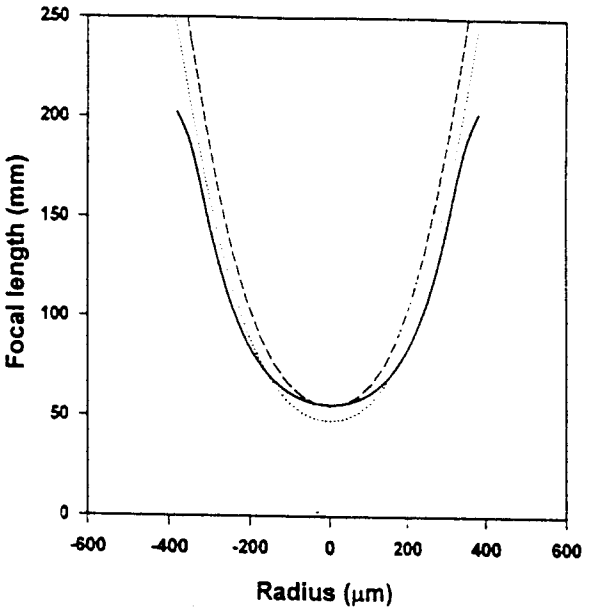

Figure 9 Radial dependence of the thermal lens focal length. (The solid line was calculated from the measured phase difference data. The dashed line represents the predicted radial dependence of focal length for a Gaussian pump beam taking into account the contribution due to the temperature dependence of refractive index only. The dotted line represents the predicted radial variation in focal length, modified to take into account the measured contributions to lensing from the stress dependence of refractive index and end-face bulging.

interferometer, and the end-face curvature, using a Michelson interferometer, we were able to show that the relative contributions to thermal lensing are approximately; 86% due to temperature dependence of refractive index, 8% due to end-face curvature and 6% due to radial stress dependence of refractive index. Taking into account these additional contributions and simply multiplying equation (19) for $f_t(0)$ by 0.86 results in a predicted focal length given by the dotted line in fig. 9, which is in good agreement with the experimental data. However, as a consequence of the Gaussian pump beam approximation the predicted values for focal length are slightly shorter than the experimental values in the centre of the pumped region.

The measured variation of lens power at r=0 with absorbed pump power for both

lasing and non-lasing conditions is plotted in fig. 10. In both cases there is a small departure from the linear dependence on pump power predicted by equation (18).

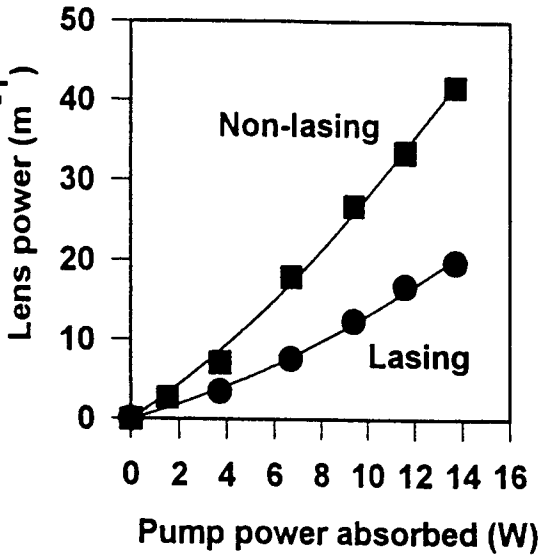

Figure 10 Thermal lens power at r=0 versus absorbed pump power under lasing and non-lasing conditions.

However the most striking feature is the ~factor-of-two stronger lensing under non-lasing conditions. A full explanation for this is not yet available, but it is thought that it is at least in part due to upconversion processes [22] leading to increased thermal loading under non-lasing conditions.

7. The Effect of Thermal Lensing on Beam Quality

The highly aberrated nature of the thermal lens can lead to significant beam distortion. In order to minimise this distortion, and hopefully achieve near to diffraction-limited operation, at high pump powers it is useful to have a quantitative model which predicts the degradation in beam quality in a given situation. In ref. 23 it is shown that a laser beam with a Gaussian intensity profile and initial beam quality factor M_i^2, after propagating through a lens of focal length f which produces a phase distortion $\Delta\phi(r)$ of the form

$$\Delta\phi(r) = \frac{2\pi}{\lambda}\left(\frac{r^2}{2f} - C_4 r^4\right) \tag{20}$$

will suffer a degradation in beam quality with the resultant beam quality factor M_f^2 being given by

$$M_f^2 = \sqrt{(M_i^2)^2 + (M_q^2)^2} \tag{21}$$

M_q^2 is the additional contribution to the beam quality factor due to the quartic phase aberration given by

$$M_q^2 = \frac{8\pi C_4 w_L^4}{\lambda\sqrt{2}} \tag{22}$$

where C_4 is the quartic phase aberration coefficient. By comparison of equations (14) and (20) it can be seen that the phase distortion caused by thermal lensing in end-pumped lasers is generally more complicated than the example considered in ref. 23. However, if we restrict our consideration to the situation where the laser beam size is small compared to the pump beam size, so that we neglect terms higher than the quartic, then M_q^2 is given by the expression:

$$M_q^2 = \left(\frac{P_p \gamma \eta_{abs} \frac{dn}{dT}}{\lambda K_c \sqrt{2}}\right)\left(\frac{w_L^4}{w_p^4}\right) \tag{23}$$

The above expression indicates that in addition to its dependence on the power dissipated as heat and the thermo-optical and thermo-mechanical properties of the laser material, the degradation in beam quality also depends very strongly on the ratio of the laser beam radius to the pump beam radius. If $w_L \ll w_p$, then the beam quality is less strongly influenced by thermally-induced aberrations, and in the limit where $w_L/w_p \to 0$, then $M_q^2 \to 1$. However, if $w_L \geq w_p$ then even a weakly aberrated lens can result in a marked

degradation in the beam quality. The physical explanation for this is that the degradation in beam quality depends on the wavefront distortion introduced by the non-parabolic phase aberrations of the thermal lens. A laser beam with small beam radius, and hence a short Rayleigh range, will have spherical wavefronts of comparatively high curvature and hence the relative deviation in phase introduced by the aberrated thermal lens will be much smaller than would be the case for a beam with a larger radius.

One further point to note is that the presence of highly aberrated thermal lensing is not exclusive to end-pumping with high-power diodes. In fact the ability to generate strong lensing is actually determined by on the brightness of the diode pump source. Low power diodes are generally much brighter than high-power diode-bars, and hence can produce very strong and highly aberrated thermal lensing. The fact that there has been little degradation in laser beam quality observed in low power diode-pumped lasers is actually because typical pump beam sizes, and hence the laser mode sizes employed, tend to be rather small, resulting in a much shorter Rayleigh range than for the larger mode sizes required for high-power pump sources. Thus the degradation in beam quality at high pump powers is actually caused by the combination of thermally-induced aberrations and the requirement for comparatively large TEM_{oo} mode sizes which have a Rayleigh range comparable to or greater than the thermal lens focal length.

8. Beam Quality Degradation and Depolarisation Loss

The above simplified model for degradation in beam quality is strictly only valid in the regime where $w_L \ll w_p$. To confirm the validity of this model and to investigate its effectiveness outside this operating regime we have performed a simple experiment to measure the increase in M^2 for a diffraction-limited laser beam after a single-pass through a diode-pumped Nd:YAG rod. The experimental arrangement (shown in fig.11), was very similar to that used for thermal lensing measurements shown in fig.7. The main difference was that the second arm of the interferometer was removed and the CCD camera replaced by a Coherent Modemaster to measure the M^2 factor. The increase in M^2 value was measured under non-lasing and lasing conditions for a series of different Nd:YLF probe beam sizes in the Nd:YAG rod.

The results of this investigation (shown in fig. 12) indicate a marked increase in the M^2 value with probe beam size, due to the effect of thermally-induced lens aberrations. It is also apparent that the M^2 values measured under non-lasing conditions are significantly worse than those measured under lasing conditions. This appears to imply appreciably greater thermal loading under non-lasing conditions (by approximately a factor of ~ 2) at high pump intensities, and is consistent with the thermal lens measurements under lasing and non-lasing conditions. The calculated value for M^2 under lasing conditions is also plotted in fig. 12. From close inspection of the data it can be seen that for good beam quality (i.e $M^2 < 1.1$), then as a rough guide we require a laser beam radius $w_o < 140\mu m$. The approximate analytical model is in reasonable agreement with the measured M^2 values up to larger beam size of $\approx 180\mu m$ (i.e. $w_L/w_p \approx 0.77$), hence it can serve as a good guide as to the maximum value for the ratio

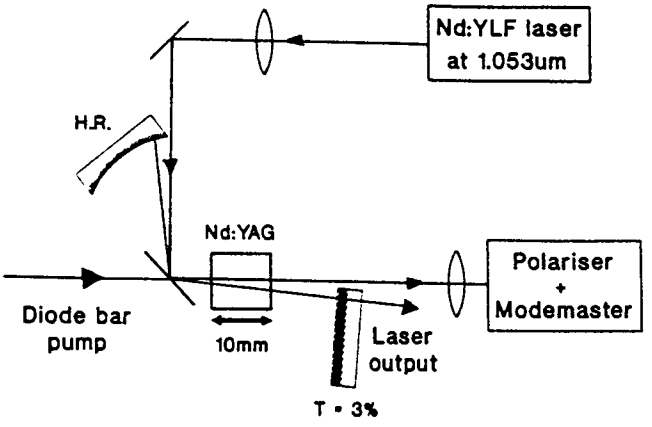

Figure 11 Experimental set-up for measuring degradation in beam quality and depolarisation loss after a single-pass through the thermal lens under lasing and non-lasing conditions.

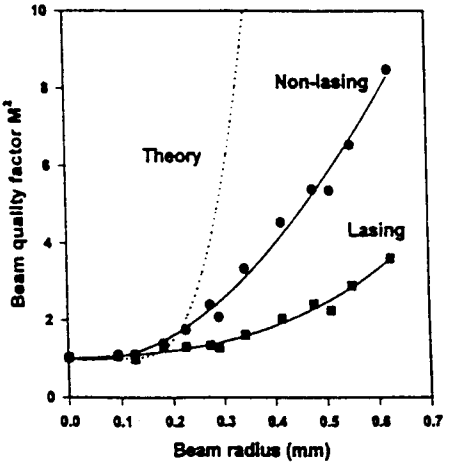

Figure 12 Single-pass degradation in beam quality versus probe beam size. The dotted line shows the beam degradation factor β for laser operation at 1.064μm.

w_L/w_p that can be used without significantly degrading the beam quality. For larger w_L the predicted values for M^2 are higher than the experimental values because the quartic phase aberration approximation gives a much larger departure from the ideal quadratic phase difference than is the case in practice.

In addition to beam quality another important factor is the depolarisation loss due to thermally-induced stress-birefringence. This depends on a number of parameters including the pump and laser beam sizes. Unfortunately, calculating the depolarisation loss for a Gaussian pump is in general rather complicated, so instead we have simply measured it using the experimental arrangement shown in fig. 11, with the Mode-master replaced by a polariser. The single-pass depolarisation loss is plotted in fig. 13 as a function of laser beam size under both lasing and non-lasing conditions. It can be seen that there is a significant increase in depolarisation loss as the laser beam size increases. Furthermore the loss is significantly higher under non-lasing conditions, which is again consistent with a factor of ~2 extra heat loading.

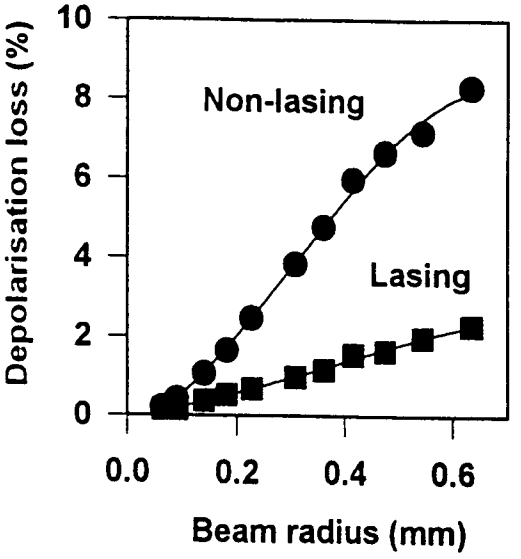

Figure 13 Single-pass depolarisation loss versus probe beam size.

9. Resonator Design Strategy

It is clear from the preceding section that in order to avoid significant degradation in beam quality and depolarisation loss for the TEM_{oo} mode at high pump power, it is necessary to use a resonator with a TEM_{oo} radius in the laser rod which is significantly smaller that the pump beam radius. This is in contrast to the situation at low powers

where it is generally accepted that one should use a resonator design with $w_L \geq w_p$ for efficient TEM_{oo} operation. At high pump powers, the smaller the ratio w_L/w_p the lower the depolarisation loss and the smaller the degradation in beam quality. Unfortunately one can not simply choose a resonator with an arbitrarily small laser mode size, since there will then be a significant amount of undepleted inversion in the pumped region not occupied by the laser mode, leading to multi-transverse mode oscillation and hence a non-diffraction-limited laser output. In practice therefore, it is necessary to use the largest possible laser mode size without significantly increasing the M^2 value and the depolarisation loss. The upper limit on the TEM_{oo} size that can be used for laser operation with for example, $M^2 < 1.1$, is difficult to calculate, but a rough value can be estimated from the experimental data on single-pass beam degradation and the discussion of the preceding section. One important question that now arises is which of the two requirements, that is, for good beam quality or low depolarisation loss, determines the upper limit on the laser mode size. For relatively high gain laser transitions, such as the $1.064\mu m$ line, a relatively high depolarisation loss $\sim 1\%$ per pass can be tolerated without causing a significant decrease in efficiency. Hence, from comparison of figs. 12 and 13, it can be seen that the requirement for good beam quality determines the upper limit on the laser mode size. However, for low gain laser transitions (e.g. the 946nm line) a much smaller depolarisation loss is required, indicating that the upper limit on the mode size is dictated by the requirement for low depolarisation loss. Regardless of the situation, the laser mode size must still be appreciably smaller than the pump beam size and hence there is still the problem of some undepleted inversion in the wings of the pumped region which can lead to lasing on higher-order transverse modes.

One solution to this problem is to simply use an aperture to discriminate against the unwanted higher-order modes. However, this has the disadvantage that it can significantly increase the loss for the fundamental mode and hence be detrimental to the efficiency. An alternative approach is to make use of the radially varying focal length of the thermal lens to provide the required discrimination. This is based on the principle that higher-order transverse modes, by virtue of their larger beam size than the TEM_{oo} mode, will see a thermal lens with an effective focal length which is longer than that seen by the TEM_{oo} beam. Hence, choosing a resonator design where the mode size decreases with increasing focal length of the thermal lens, will effectively decrease the ratio of beam sizes of the higher-order transverse modes to the TEM_{oo} mode. This results in a decrease in available gain for higher-order modes by virtue of their stronger spatial overlap with the fundamental mode, hence suppressing their oscillation.

10. Experiments on Power-scaling End-pumped Nd:YAG Lasers

To investigate the potential benefits of this approach we have performed a number of experiments on a Nd:YAG laser end-pumped by a high-power diode-bar. The pumping scheme used is identical to that described in earlier sections, delivering a maximum of 14.2W in a nearly circular beam of radius $w_p \approx 225\mu m$. The resonator design employed

was a simple folded cavity (fig. 14), consisting three mirrors; two plane mirrors, one having high transmission (>96%) at the pump wavelength (809nm) and 5% transmission at the lasing wavelength (1.064μm) and the other with a transmission of 2% at 1.064μm, and a curved high reflector of radius of curvature 100mm. The 10mm

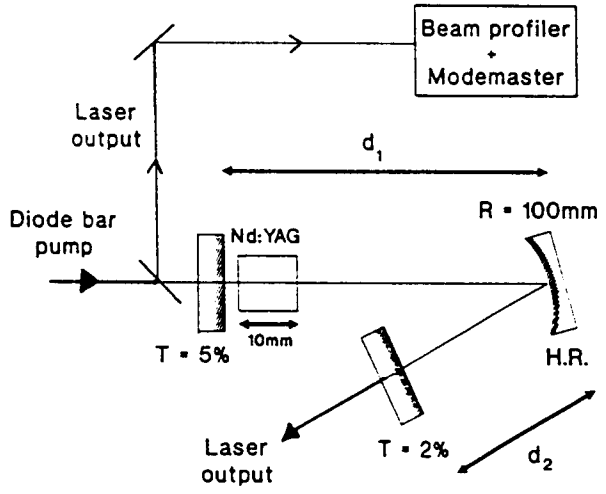

Figure 14 Resonator design for Nd:YAG laser experiments.

long Nd:YAG laser rod was mounted, as before, in a water-cooled copper heat-sink in close proximity to the pump input mirror. The use of two output couplers facilitated simultaneous monitoring of the laser output power, beam quality factor and transverse intensity profile of the output beam, whilst having the additional advantage of allowing easy determination of the laser mode size at the pump input mirror, and hence in the laser rod, without a knowledge of the resonator design and the effect of the thermal lens. This simple folded cavity, by varying the distances d_1 and d_2 between the curved mirror and the two plane mirrors, provided enough flexibility in resonator design to allow a detailed investigation of the requirements for efficient TEM_{oo} operation.

Using the standard ABCD matrix formalism for resonator design [24], it can be shown that the requirement for a decrease in laser mode size in the rod with increasing focal length of the thermal lens can be realised in this simple folded cavity (fig. 14) by choosing an effective optical length for arm 1 to be just less than the sum of the focal lengths of the curved high reflector and the thermal lens focal length ($\sim$60mm at the maximum pump power). In our experiment the length d_1 was set to 109mm with the angle of incidence on the curved mirror made small (<5°) to render the effects of astigmatism negligible. The avoidance of astigmatism is a particularly important aspect of the resonator design given that the requirement for a large decrease in laser mode size with increasing thermal lens focal length typically implies, as in this case, operating

close to the edge of stability. Thus in addition to using a small angle of incidence on the curved mirror, it is also important to avoid any astigmatism in the thermal lensing, due to, for example, an elliptical pump beam or a pump beam with M^2 values in orthogonal planes which differ significantly. Having set the value for d_1 to give the required resonator response to the varying thermal lens focal length, the required TEM_{∞} size in the laser rod can be obtained by simply adjusting the arm length d_2. Calculated values for the TEM_{∞} beam radius at the laser rod are plotted as a function of thermal lens focal length for different values of d_2 in fig. 15. Without a polariser present in the

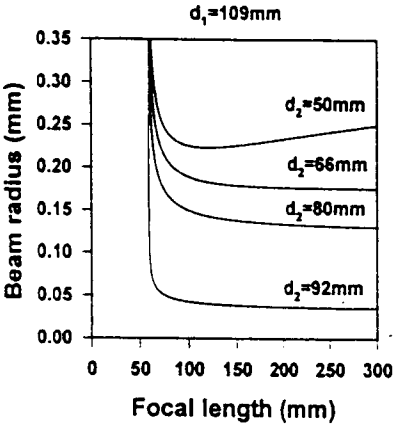

Figure 15 TEM_{∞} radius versus arm length d_2.

cavity and at the maximum available pump power of 14.2W, it was found that TEM_{∞} operation ($M^2 \leq 1.1$) could in practice be achieved for a small range of values d_2 of approximately (70 ± 0.5)mm, resulting in a maximum output power of 6.2W (fig.16). Inserting a Brewster-angled plate into the cavity resulted in a linearly polarised, TEM_{∞} output ($M^2 < 1.1$) of slightly lower output power 5.5W, the reduction caused by an additional cavity loss of $\sim 1\%$ due to thermally-induced stress birefringence. This depolarisation loss is consistent with our expectations based on the experimental data for single-pass depolarisation loss (fig. 13) and the measured laser mode radius of 165μm, which is significantly smaller than the pump beam radius. One interesting observation was that the reliability of TEM_{∞} operation was improved as a result of including a polariser in the cavity and additionally, had the benefit of extending the range of arm lengths d_2, and hence the range of laser mode sizes, over which near diffraction-limited operation can be maintained. This can be attributed to the additional transverse mode discrimination provided by the polariser by virtue of the fact that higher-order transverse modes with larger beam sizes see, on average, a larger stress-induced birefringence and hence experience increased depolarisation loss at the polariser compared to the smaller

fundamental mode. However, as expected for both polarised and unpolarised lasers, diffraction-limited beam quality could only be maintained for a small range of pump powers (typically <4W) close to the maximum power. At lower powers the laser mode size is reduced, due to the weaker thermal lens, hence the laser operates on many transverse modes. However, TEM_{∞} mode operation could in principle be maintained over the full power range by careful selection and positioning of an aperture designed to strongly discriminate against higher-order transverse mode oscillation at low pump powers, while, by virtue of the change in laser modes size with increasing pump power, providing less discrimination at high powers. In this way the laser efficiency at high powers would not be affected. However, this approach would still have the disadvantage that the laser beam size and divergence would change with pump power. Thus for some applications simply operating at the maximum pump power and using an external attenuator to vary the power might prove to be a more attractive alternative.

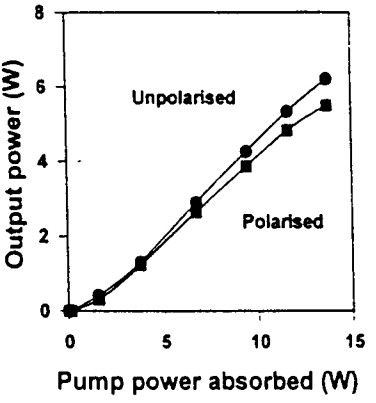

Figure 16 Nd:YAG laser output power at 1.064μm versus absorbed pump power.

To provide additional confirmation of the benefits of this resonator design approach, and in particular, to demonstrate the importance of using a resonator with a laser mode size which decreases with increasing thermal lens focal length, we have also investigated the behaviour of a similar folded cavity, but this time with arm lengths d_1 and d_2 selected to give a laser mode radius similar to that used in the previous experiment (i.e. $\sim$165μm), but one which does not vary appreciably with rod focal length. At the maximum available pump power, a folded cavity with $d_1 \approx 80$mm and $d_2 \approx 50$mm roughly satisfies these requirements. This type of resonator might be have been considered as an attractive choice for a laser whose output characteristics (beam size and divergence) would not be strongly influenced by thermal lensing. However in practice

the minimum M^2 beam quality factor attainable for this resonator configuration was >2. This serves to illustrate the importance of using a resonator which satisfies both of our design criteria, namely that the TEM_{oo} size should be significantly less than the pump beam size and that the laser mode size should decrease with increasing thermal lens focal length.

This design strategy has been successfully applied to other diode-bar-end-pumped Nd:YAG lasers operating on lower gain transitions at 946nm [9] and at 1.3μm [25], yielding diffraction-limited performance up to power levels of 2.7W and 3.2W respectively. However, due to their relatively low gain, both of these lasers when operated with Brewster plate polarisers, provided significantly lower powers due to the depolarsiation loss resulting from thermally-induced birefringence. In the case of the 946nm Nd:YAG laser a maximum polarised output of 2.1W, and for 1.3μm operation, a maximum linearly polarised output of ~1.75W were achieved. In the latter case the much higher heat loading density, which results from the larger quantum defect, makes it more difficult to achieve an efficient, linearly polarised TEM_{oo} output.

11. Power-scaling Limit

The ultimate limit to power-scaling of any laser is essentially determined by the stress-fracture limit. However, there are numerous brightness-dependent applications in areas such as non-linear optics and materials processing where scaling to high powers must be achieved without significant degradation in beam quality. In this case, given that there are numerous techniques for the compensation of thermally-induced stress-birefringence, it is in fact beam quality degradation due to the highly aberrated thermal lensing which effectively limits the maximum power that can be achieved. The strategy for resonator design described in section 9 provides a means for reducing the effects of the aberrated lens on beam quality, but it does not allow indefinite power-scaling with the maintenance of diffraction-limited beam quality. We can establish a very rough guide to the maximum power-scaling limit by requiring that $M_q^2 \leq 0.46$ (corresponding to $M^2 \leq 1.1$). The net result, obtained from equation (23), is that the maximum pump power used P_{pmax} must satisfy the following condition for good beam quality:

$$P_{pmax} \leq \frac{0.65 K_c \lambda}{\rho^4 \gamma \eta_{abs} \frac{dn}{dT}} \qquad (24)$$

where $\rho = w_L/w_p$. It should be noted however that the above condition is only a rough guide, since it considers only a single-pass through the laser rod, and is only valid for $w_L \ll w_p$. It might appear from (24) that the maximum useful pump power is independent of the actual pump beam and laser mode size, and is only dependent on their ratio. At first sight this seems counter-intuitive since one might have expected a

limit dependent on pump intensity, which would have then allowed further power-scaling by simply using a larger beam pump beam size. However, the explanation for this is as follows: Using a larger pump beam size to reduce the pump intensity, and hence the phase aberration, would also necessitate the use of a larger laser mode size to allow efficient extraction of the gain, which would have a longer Rayleigh range. Given that beams with a longer Rayleigh range are more susceptible to beam distortion via phase aberrations, the net result of increasing the pump beam size would be to leave the value for M^2 approximately unchanged. Thus, from the point of view of optimising the laser efficiency it could be argued that it is in fact much better to use the smallest possible pump beam size, and hence laser mode size, to allow efficient utilisation of the inversion in the wings of the pumped region. Obviously, this requires a high-power diode pump source with reasonably good beam quality. The main disadvantage of intense pumping however is that, due to the very strong thermal lensing which results, TEM_{00} operation can only be maintained over a very small power range without the use of apertures.

Fig.17 gives a rough guide to the maximum pump power that can be used for a diode-pumped Nd:YAG laser at $1.064\mu m$ with different values of ρ. This indicates that the condition $w_L \geq w_p$ for good beam quality at low pump powers becomes invalid for pump powers in excess of a few watts. Thus to avoid significant TEM_{00} beam distortion

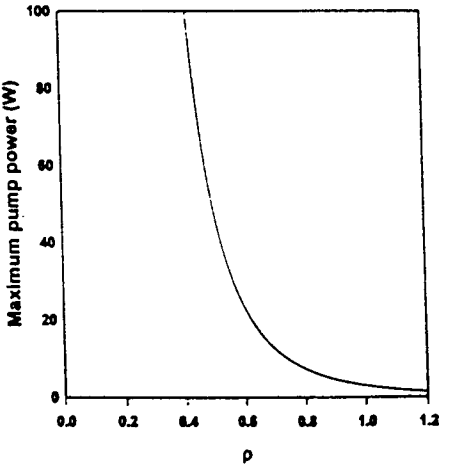

Figure 17 Rough guide to the maximum incident pump power for low TEM_{00} beam degradation as a function of ρ.

when scaling to higher pump powers it is necessary to use progressively smaller values for ρ. However, if the ratio ρ is too small then the undepleted inversion in the wings of the pumped region leads to multi-transverse operation, even when using a resonator selected to satisfy the condition that the TEM_{00} mode size decreases with increasing

thermal lens focal length. Under these conditions an aperture is required to provide the extra discrimination to prevent oscillation on higher-order modes. However, since the TEM_{oo} intensity is very low in the wings of the pumped region it is difficult to utilise the undepleted inversion, hence the efficiency decreases. The implication of this is that there is a very definite power-scaling limit for diffraction-limited end-pumped solid-state lasers due to thermal lensing. For a Nd:YAG laser operating at $1.064\mu m$ employing an edge-cooled rod geometry and no compensation of the phase aberration, this limit is probably less than $\sim$20W. This is well below the maximum multimode output power achievable.

12. Power-scaling with Nd:YLF

One approach to allow further power-scaling, without resorting to a change of heat-sink configuration or the use of compensating components for the phase aberration, is to use laser materials which have characteristics better suited to operation at high powers. One laser material which has recently received growing interest is $Nd:YVO_4$. The main attraction of $Nd:YVO_4$, apart from its natural birefringence, is its high $\sigma\tau_f$ product, which is $\sim$factor-of-two times larger than for Nd:YAG at $1.064\mu m$, and its short absorption length ($<$1mm) for diode pump light at $\sim$809nm. The latter allows for much tighter focusing of the pump source allowing the use of a relatively small laser mode size. Its low saturation intensity in combination with the use of a small mode size allows for better extraction of the gain in the wings of the pumped region and hence the use of resonator designs with smaller values of ρ, thus allowing scaling of TEM_{oo} operation to higher powers (e.g. [1]). The main disadvantage of $Nd:YVO_4$ however, is that it exhibits quite strong thermal lensing, comparable to Nd:YAG, thus making it difficult to ensure TEM_{oo} operation of the full range of pump power without the use of apertures.

An alternative laser material which offers some attractions for further power-scaling is Nd:YLF. In addition to its natural birefringence, Nd:YLF has the attraction that on the σ-polarisation (corresponding to $1.053\mu m$ operation) the thermal lensing is very weak. This is due to the combination of a small, negative value for dn/dT (i.e. -2×10^{-6}) and a positive contribution to thermal lensing from end-face bulging which substantially offsets the negative lensing. The net result is that, for the same thermal loading density, the thermal lensing on the $1.053\mu m$ transition in Nd:YLF is $\sim$six times weaker than in Nd:YAG. However Nd:YLF suffers from the problem that it has a stress-fracture limit which is $\sim$five times lower than Nd:YAG. This has all but limited operation of Nd:YLF lasers in cw end-pumped configurations to relatively low powers. However, with new beam shaping techniques, such as the two mirror beam shaper [8], which have led to higher brightness pump beams, a solution to the fracture problem is now presented. This involves using a longer Nd:YLF rod and distributing the absorbed pump power over a longer length by detuning the pump wavelength from the absorption peak, or using a rod with lower Nd^{3+} concentration. The pump beam with its improved beam quality, can be focused to a relatively small beam, but with a long Rayleigh

range, $z_{op}=\pi n w_p^2/M^2\lambda$, chosen to be comparable to or greater than the absorption length for the pump. In this way the pump beam size is kept reasonably constant over the length of the Nd:YLF crystal. Previously to adopting this strategy, the 1% Nd-doped YLF crystals employed in our experiments were found to fracture for diode pump powers in the range of 10W to 14W, when using pump beam radius of $\sim 300\mu$m. Using a 0.5% Nd-doped YLF crystal of length 15mm and a wavelength slightly detuned from the peak absorption, results in an effective absorption length for diode-bar pump radiation at ~ 792nm of approximately 6mm. This allows end-pumping through opposite end-faces of the Nd:YLF crystal by two 20W diode-bars whose outputs, each using a two-mirror beam shaper, could be focussed to beam sizes of $\sim 300\mu$m, without the risk of fracture. Using this approach we have demonstrated >11W of cw output at 1.053μm in a TEM_{oo} beam with $M^2<1.1$. The attraction of this approach is that due to the relatively weak thermal lensing, the laser mode size in a typical folded-cavity varies very little (by less than 10%) over full range of pump power. This allows for much more flexibility in resonator design, since the phase aberration is relatively small. As a demonstration of this we have also constructed a Nd:YLF ring laser end-pumped in a similar fashion by two 20W diode bars resulting in >10W of single-frequency output at 1.053μm, and an intracavity-frequency-doubled version (using LBO) with a single-frequency green output at 526.5nm of 6.2W, which corresponded to 8.5W of green generated internally in the Brewster-angled LBO crystal [26]. Further reduction in the Nd^{3+} concentration, improvements in pump beam quality and the use of multiple rod geometries should allow significant further scaling of TEM_{oo} power, without the risk of fracture. Thus Nd:YLF promises to be an attractive alternative to laser materials such as Nd:YAG and Nd:YVO_4 for high-power end-pumped solid-state lasers.

13. Conclusions

In end-pumped solid-state lasers employing edge-cooled rod geometries, thermal lensing, rather than stress-induced fracture, appears to present the most difficult obstacle to the scaling of diffraction-limited performance to high power levels. This is a consequence of degradation in laser beam quality due to the highly aberrated nature of the thermal lens. To reduce the effect of these non-parabolic phase aberrations we have proposed an alternative design strategy where the resonator must satisfy two conditions, which are that the TEM_{oo} mode size must be significantly smaller than the pump beam size and that the TEM_{oo} size must decrease with increasing thermal lens focal length. This resonator design approach is in stark contrast with the approach that is generally adopted for lower power lasers. We have also postulated that for this end-pumped edge-cooled geometry there is an upper power limit on a given laser transition for diffraction-limited operation. This limit depends on a number of factors including the characteristics of the laser material, and we have shown that if care is taken to avoid thermally-induced fracture, then Nd:YLF operating at 1.053μm has some advantages over Nd:YAG and Nd:YVO_4, due to its superior thermo-optical properties. However, indefinite scaling in the diffraction-limited output from end-pumped lasers can only be achieved if measures are taken to compensate for the thermally-induced aberrations [2].

14. References

1. Nighan, W. L., Dudley, D. and Keirstead, M. (1995) Diode-bar-pumped Nd:YVO_4 lasers with >13W TEM_{∞} output at >50% efficiency, *Conference on Lasers and Electro-Optics, Vol. 15, OSA Technical Digest Series, (Optical Society of America, Washington, D.C.)*, 17.
2. Tidwell, S. C., Seamens, J. F., Bowers, M. S. and Cousins, A. (1992) Scaling cw diode-end-pumped Nd:YAG lasers to high average powers, *IEEE J. Quantum Electron.* **28**, 997-1009.
3. Zbinden, H. and Balmer, J. E. Q-switched Nd:YLF laser end-pumped by a diode-laser-bar, *Opt. Lett.* **15**, 1014-1016.
4. Graf, Th. and Balmer, J. E. High-power Nd:YLF laser end-pumped by a diode-laser bar, *Opt. Lett.* **18**, 1317-1319.
5. Kierstead, M. S. and Baer, T. M.(1991) 10W TEM_{∞} output from a diode-pumped, solid-state laser, *Conf. Lasers and Electro-Optics, OSA Technical Digest Series, vol. 10, (Optical Society of America, Washington, D.C.)*, 490.
6. Leger, J. R. and Goltsos, W. C. (1995) Geometrical transformation of linear diode-laser arrays for longitudinal pumping of solid-state lasers, *IEEE J. Quantum Electron.* **28**, 1088-1100.
7. Yamaguchi, S., Kobayashi, T., Saito, Y. and Chiba, K. (1995) Collimation of emissions from a high-power multistripe laser-diode bar with multiprism array coupling and focusing to a small spot, *Opt. Lett.* **20**, 898-900.
8. Clarkson, W. A. and Hanna, D. C. (1996) Two-mirror beam-shaping technique for high-power diode bars, *Opt. Lett.* **21**, 375-377.
9. Clarkson, W. A., Koch, R. and Hanna, D. C. (1996) Room-temperature diode-bar-pumped Nd:YAG laser at 946nm, *Opt. Lett.* **21**, 737-739.
10. Brauch, U., Giesen, A., Karszewski, M., Stewen, C. and Voss, A. (1995) Multiwatt diode-pumped Yb:YAG thin disc laser continuously tunable between 1018 and 1053nm, *Opt. Lett.* **20**, 713-715.
11. Kubodera, K. and Otsuka, K. (1977) Diode-pumped miniature solid-state laser: design considerations, *Appl. Opt.* **16**, 2747-2752.
12. Laporta, P. and Brussard, M. (1991) Design criteria for mode size optimisation in diode-pumped solid-state lasers, *IEEE J. Quantum Electron.* **27**, 2319-2326.
13. Kubodera, K, and Otsuka, K. (1979) Single-transverse-mode $LiNdP_4O_{12}$ slab waveguide laser, *J. Appl. Phys.* **50**, 653-659.
14. Clarkson, W. A. and Hanna, D. C. (1989) Effects of transverse mode profile on slope efficiency and relaxation oscillations in a longitudinally-pumped laser, *J. mod. Opt.* **36**, 483-498.
15. Fan, T. Y. and Byer, R. L. (1987) Modeling and cw operation of a quasi-three-level 946nm Nd:YAG laser, *IEEE J. Quantum Electron.* **23**, 605-612.
16. Risk, W. P. (1988) Modeling of longitudinally-pumped solid-state lasers exhibiting reabsorption losses, *J. Opt. Soc. Am. B*, **5**, 1412-1423.
17. Koechner, W. (1988) *Solid-State Laser Engineering*, Springer-Verlag, New York, pp. 344.
18. Lu, G., Kugler, N., Weber, H., Dong, S., Muller, N. and Wittrock, U. (1996) A novel approach for compensation of birefringence in cylindrical Nd:YAG rods, *Optical and Quantum Electronics*, **28**, 75-69.
19. Innocenzi, M. E., Yura, H. T., Fincher, C. L. and Fields, R. A. (1990) Thermal modeling of continuous-wave end-pumped solid-state lasers, *Appl. Phys. Lett.* **56**, 1831-1833.
20. Kaminskii, A. A. (1989) *Laser crystals*, Springer-Verlag, New York, pp.321.
21. Fan, T. Y. (1993) Heat generation in Nd:YAG and Yb:YAG, *IEEE J. Quantum Electron.* **29**, 1457-1459.
22. Guyot, Y., Manaa, H., Rivoire, J. Y., Moncorge, R., Garnier, N., Descroix, E., Bon, M. and Laporte, P. (1995) Excited-state-absorption and upconversion studies of Nd^{3+}-doped single crystals $Y_3Al_5O_{12}$, $YLiF_4$ and $LaMgAl_{11}O_{19}$, *Phys. Rev. B*, **51**, 784-799.
23. Siegman, A. E. (1993) Analysis of laser beam quality degradation caused by quartic phase aberrations,

Appl. Opt. **32**, 5893-5901.

24. Kogelnik, H. and Li, T. (1966) Laser beams and resonators, *Appl. Opt.* **5**, 1550-1567.
25. Kern, M. A., Clarkson, W. A. and Hanna, D. C. (1997) Resonator design considerations for high-power TEM_{00} operation of a Nd:YAG laser at 1.3μm end-pumped by a diode-bar, *Conference on Lasers and Electro-Optics, Vol. 11, OSA Technical Digest Series, (Optical Society of America, Washington, D.C.),* 479.
26. Hardman, P. J., Clarkson, W. A., Martin, K. I., Butterworth, S. D. and Hanna, D. C. (1997) Mode-hop-free tuning in high-power intracavity-frequency-doubled Nd:YAG and Nd:YLF ring lasers, *Conference on Lasers and Electro-Optics, Vol. 11, OSA Technical Digest Series, (Optical Society of America, Washington, D.C.),* 520.